

Operando NAP-XPS unveils differences in MoO₃ and Mo₂C during hydrodeoxygenation

Karthick Murugappan¹, Eric M. Anderson¹, Detre Teschner^{2,3}, Travis E. Jones², Katarzyna Skorupska^{2,3}, and Yuriy Román-Leshkov^{1*}

MoO₃ and Mo₂C have emerged as remarkable catalysts for the selective hydrodeoxygenation (HDO) of a wide range of oxygenates at low temperatures (i.e., ≤ 673 K) and H₂ pressures (i.e., ≤ 1 bar). While both catalysts can selectively cleave C–O bonds, the nature of their active sites remains unclear. Here, we used operando near-ambient pressure X-ray photoelectron spectroscopy to reveal important differences in the Mo 3d oxidation states between the two catalysts during the HDO of anisole. This technique revealed that although both catalysts featured a surface oxycarbide phase, the oxygen content and the underlying phase of the material impacted the reactivity and product selectivity during HDO. MoO₃ transitioned between 5+ and 6+ oxidation states during operation, consistent with an oxygen vacancy driven mechanism wherein the oxygenate is activated at undercoordinated Mo sites. In contrast, Mo₂C showed negligible oxidation state changes during HDO, maintaining mostly 2+ states throughout the reaction.

Introduction

Hydrodeoxygenation (HDO) is an important upgrading strategy for converting lignocellulosic biomass to fuels and chemicals that relies on molecular H₂ to selectively remove oxygen in the form of water.^{1–13} While noble metal catalysts have dominated the HDO landscape, molybdenum trioxide (MoO₃)^{14–20} and molybdenum carbide (Mo₂C)^{21–31} have recently emerged as promising earth-abundant alternatives that can selectively cleave C–O bonds under mild conditions. In contrast to state-of-the-art noble metal catalysts, MoO₃ and Mo₂C catalysts produce unsaturated hydrocarbons, while concurrently minimizing both the saturation of C=C double bonds and the cleavage of C–C bonds.

Román-Leshkov *et al.* showed that MoO₃ converts a wide-range of linear and aromatic oxygenates into olefinic and aromatic hydrocarbons, respectively, with high selectivities (>97%) using low H₂ pressures (≤ 1 bar) and temperatures below 673 K.¹⁴ Post-reaction characterization studies revealed that MoO₃ underwent partial carburization to form an oxycarbohydride (MoO_xC_yH_z) featuring a large proportion of Mo⁵⁺ surface species.¹⁵ It was hypothesized that these undercoordinated species (i.e. oxygen vacancies) were responsible for activating the C–O bond and that the lattice carbon in MoO_xC_yH_z played a crucial role in preventing the over-reduction of Mo⁵⁺ into less active Mo⁴⁺ sites.¹⁵

In parallel, Bhan and co-workers showed that Mo₂C is highly selective for cleaving strong phenolic C–O bonds at atmospheric H₂ pressures and temperatures ranging from

420 to 553 K.^{22, 23, 26, 28, 29} For instance, Mo₂C converted anisole to benzene with selectivity values >90% at 423 K. Detailed kinetic studies revealed that two distinct sites are required: one for H₂ dissociative adsorption and one for oxygenate activation.^{22, 26, 29} The site required for oxygenate adsorption was hypothesized to be metal-like in nature based on the invariant product generation rates when normalized by *ex situ* CO chemisorption.^{22, 26} In a subsequent study, an oxygen mass balance performed during transient HDO experiments revealed oxygen incorporation equivalent to ~0.29 monolayers.²⁷ Given the lack of bulk structural changes, this oxidation was hypothesized to be a surface and/or a subsurface phenomenon.^{26–29}

Notwithstanding this evidence, the exact nature of the active sites in both materials remains unresolved. On the one hand, the presence of oxycarbide sites may suggest a common HDO pathway for both materials. Indeed, although CO chemisorption is typically used to titrate metallic sites that may be present in Mo₂C and not in MoO₃, CO can also bind to the undercoordinated sites of MoO_xC_yH_z.²⁷ Hence, the potential active site for oxygenate adsorption in Mo₂C could be either metallic or an oxygen vacancy similar to that observed over MoO₃. On the other hand, reactivity data has shown different HDO product distributions for both materials when compared at identical conditions (Supplementary Fig. 1), thus suggesting different site speciation over the catalytic surfaces.

Unfortunately, *ex situ* characterization techniques do not allow us to establish clear structure-performance relationships for these materials. Although post-reaction

¹Department of Chemical Engineering, Massachusetts Institute of Technology, Cambridge, Massachusetts 02139, United States. ²Fritz-Haber-Institut der Max-Planck-Gesellschaft, Abteilung Anorganische Chemie, Berlin 14195, Germany. ³Max-Planck-Institut für Chemische Energiekonversion, Stiftstr. 34–36, 45470 Mülheim a. d. Ruhr, Germany. *e-mail: yroman@mit.edu

X-ray photoelectron spectroscopy (XPS) of spent MoO_3 provided insights into the nature of the catalysts after reaction, this *ex situ* approach does not capture the dynamics of the catalyst surface under the reaction conditions.³² More importantly, Mo_2C is highly oxophilic, and readily forms an oxide passivation layer when exposed to O_2 .³³⁻³⁵ This changes the surface structure from that present during reaction and convolutes data from *ex situ* characterization methods.³⁴ Since both catalysts undergo significant structural and surface modifications during the course of the reaction, an *in situ* surface characterization technique is required to interrogate the active sites responsible for HDO.

Here, we used operando near-ambient pressure XPS (NAP-XPS) to probe the nature of active sites over MoO_3 and Mo_2C catalysts during HDO of anisole at 593 K and H_2 pressures (≤ 1 mbar). Using synchrotron radiation, we were able to increase surface sensitivity by modulating the incident photon energies to measure ejected photoelectrons at lower kinetic energies than those that measured with traditional ultra-high vacuum (UHV) XPS.³² Our study revealed that both catalysts predominantly produced benzene as the major product under the reaction conditions investigated. However, the changes in Mo 3d oxidation states during HDO were drastically different across both materials. The Mo 3d core level spectra were rigorously analysed with the aid of density functional theory (DFT) calculations to identify the various contributions associated with different chemical environments. In addition to Mo 3d spectra, O 1s, C 1s, surface elemental composition, C-Mo and O-Mo ratios were examined to gain insight into the cause of deactivation. Thus, our work provides a robust framework for interpreting Mo 3d XPS data for MoO_3 and Mo_2C catalysts.

Results

NAP-XPS measurements. In order to investigate the nature of the active sites during HDO, NAP-XPS measurements were performed over both MoO_3 and Mo_2C samples under identical reaction conditions ($P_{\text{total}} = 1$ mbar with $P_{\text{anisole}} = 0.005$ mbar and balance H_2 at 593 K). Due to the lack of reliable fitting strategies for surface-sensitive Mo 3d spectra for Mo_2C , DFT calculations were used to aid in developing a robust fit parameter set. In short, we benchmarked our theoretical approach first by simulating known Mo 3d line shapes of metallic Mo and MoO_2 , followed by calculating the line shape of Mo_2C (see Supplementary Methods I, Supplementary Fig. 2 and Supplementary Table 1).

Figure 1a shows the Mo 3d XPS spectra acquired over pre-reduced MoO_3 during reaction. Detailed information about Mo 3d binding energies, deconvolution parameters and a sample deconvoluted spectrum are available in the Supplementary Information (Supplementary Methods II, Supplementary Tables 1-3, and Supplementary Fig. 3). In the first 3.6 h, there is a clear continuous oxidation of Mo^{5+} to Mo^{6+} , as seen by the lower intensities of Mo^{5+} peaks and the sharper Mo^{6+} peaks. Interestingly, after *ca.* 4 h on stream, the proportion of Mo^{6+} started to decline with a concomitant increase of Mo^{5+} , ultimately reaching a steady state. No peaks correspond-

ing to Mo^{2+} (Mo_2C) or Mo (Mo metal) were observed. The distribution of Mo oxidation states was tracked as a function of time as seen in Figure 1b. Specifically, the proportion of Mo oxidation states changed from 39% Mo^{5+} and 58% Mo^{6+} to 11% Mo^{5+} and 76% Mo^{6+} in the first 3.3 h, before reaching a steady state distribution of 31% Mo^{5+} and 61% Mo^{6+} . Similarly, Mo^{4+} mirrored the trends observed with Mo^{6+} increasing from ~3% to 13% in the first 3.3 h, before decreasing to a steady state composition of ~8% Mo^{4+} species. A repeat of the experiment with a new MoO_3 pellet resulted in similar trends (Supplementary Figs. 6-8).

Control experiments on fresh MoO_3 samples were used to gain insights into the observed changes in Mo oxidation states during HDO. First, the Mo 3d spectra of untreated MoO_3 (i.e. not pretreated with H_2) acquired at 593 K in 1 mbar N_2 flow predominantly featured a combination of Mo^{6+} and Mo^{5+} states with their respective $3d_{5/2}$ peaks located at 232.8 eV³⁶ and 231.5 eV³⁶⁻³⁸ (Supplementary Fig. 9). The presence of Mo^{5+} species indicates that the sample underwent partial thermal reduction. Bulk MoO_2 (Supplementary Fig. 10) featured oxidation states corresponding to Mo^{4+} (52%), with additional contributions of Mo^{5+} (23%) and Mo^{6+} states (25%). Although most reports typically model Mo^{4+} as one set of doublet peaks,^{38, 39} recent surface science literature has shown that Mo^{4+} actually consists of 2 pairs of doublets with one narrow, asymmetric pair associated with a screened metallic environment, and one broader, more symmetric pair corresponding to an unscreened environment.⁴⁰⁻⁴² Here, we also associated the Mo^{4+} state to 2 sets of doublets with their Mo $3d_{5/2}$ peaks located at *ca.* 229.3 and 230.6 eV. Next, a pre-reduced MoO_3 sample exposed to only H_2 gas (i.e. in the absence of anisole) at 593 K showed a decreasing proportion of Mo^{6+} species from *ca.* 67% to 61% with a concomitant increase in Mo^{5+} from *ca.* 32% to 38% in the first 2.2 h, before approaching a steady state distribution of *ca.* 36% Mo^{5+} and 62% Mo^{6+} thereafter (Supplementary Figs. 11, 12).

The HDO of anisole was investigated over Mo_2C after it was treated for 3 h with H_2 at 593 K (Supplementary Fig. 13). This pre-reduction was necessary to remove any surface oxides formed during sample handling and loading pre-reaction (*vide infra*). In stark contrast to the Mo 3d spectra of pre-reduced MoO_3 , no significant changes were observed in the Mo oxidation states over Mo_2C during the course of the HDO reaction (see Fig. 2a). The distribution of Mo species remained relatively constant at *ca.* 84% Mo^{2+} , 14% Mo^{4+} , 1% Mo^{5+} and 1% Mo^{6+} (see Fig. 2b) throughout the reaction (~7 h), and resembled that obtained after the H_2 reduction. A repeat experiment with a new Mo_2C pellet showed similar trends (Supplementary Figs. 14-17). A control experiment with fresh Mo_2C in the presence of just H_2 (i.e., in the absence of anisole) was performed prior to the HDO experiment to determine the Mo 3d binding energies corresponding to Mo_2C . The corresponding Mo 3d binding energies, deconvolution fit parameters and a representative deconvoluted spectrum for Mo_2C are shown in the Supplementary Information (Supplementary Methods II, Supplementary Tables 1, 4-5 and Supplementary Fig. 4). Although most reports associate Mo^{2+} in Mo_2C with a single set of

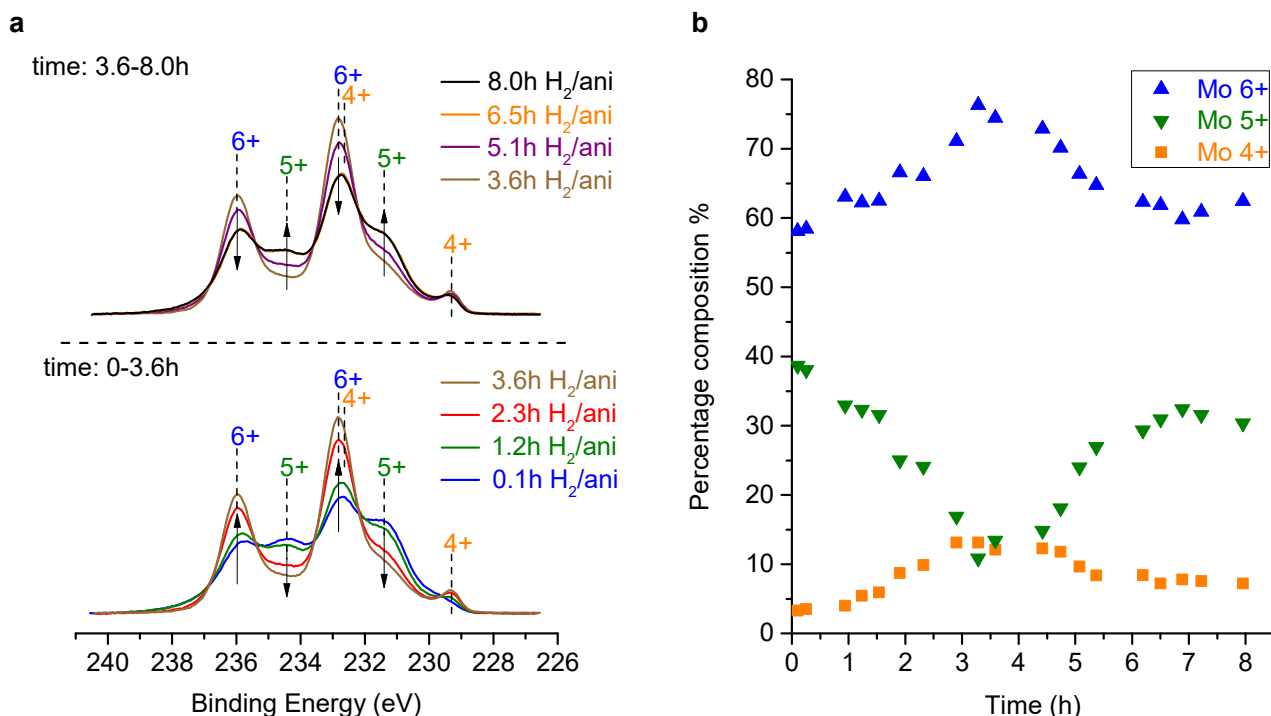


Fig. 1 | NAP-XPS of pre-reduced MoO₃ during HDO of anisole at photon energy of 473 eV. **a**, Normalized Mo 3d spectra at few selected time points from the entire data set for better visualization **b**, Percent composition of Mo oxidation states with time. Reaction conditions: T = 593 K, P_{total} = 1 mbar (P_{anisole} = 0.005 mbar, balance H₂).

doublet, our theoretical analysis (Supplementary Fig. 2) showed that Mo²⁺ features three sets of doublets. The dominant doublet corresponding to Mo²⁺ is strongly asymmetric in nature and corresponds to the Mo 3d_{5/2} signal at 228.2 eV (Supplementary Fig. 18a), in agreement with prior literature reports.^{43, 44} In addition, two minor doublets with their Mo 3d_{5/2} bands centred at ca. 228.9

and 231.9 eV also correspond to Mo²⁺ (Supplementary Fig. 4). Despite our attempts to minimize air exposure, a ca. 0.33 nm thick oxide overlayer (see Supplementary Methods III, Supplementary Table 6) exists on the 'fresh' Mo₂C surface as evidenced by the presence of a broad shoulder in the Mo 3d spectra at higher binding energies. Peak deconvolution revealed that ca. 72% of Mo species exist as

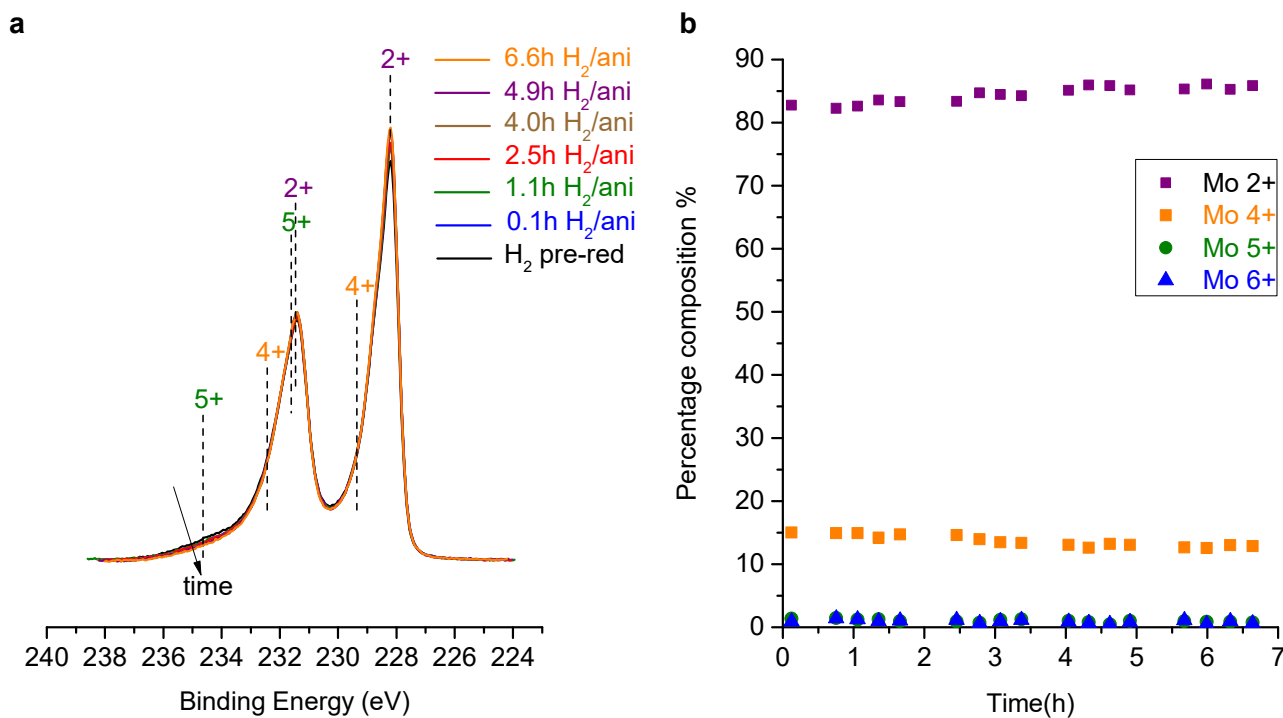


Fig. 2 | NAP-XPS of Mo₂C during HDO of anisole at photon energy of 473 eV. **a**, Normalized Mo 3d spectra at few selected time points from the entire data set for better visualization **b**, Percent composition of Mo oxidation states with time. Reaction conditions: T = 593 K, P_{total} = 1 mbar (P_{anisole} = 0.005 mbar, balance H₂) and H₂ pre-reduction = 3 h.

Mo²⁺, associated with carbidic Mo₂C, while Mo⁴⁺, Mo⁵⁺ and Mo⁶⁺ constitute the remaining 15%, 10% and 3% respectively, associated with oxidic species. We note that a conservative Mo₂C fitting was performed wherein the asymmetry parameter of the dominant Mo²⁺ peak was not allowed to be too high to obtain reasonable fits, thus potentially underestimating the Mo²⁺ and overestimating the higher oxide contributions. The presence of residual oxygen on freshly synthesized Mo₂C was also observed by Bhan and co-workers.²⁹ The intense carbidic C 1s signal at ca. 283.1 eV⁴⁵⁻⁴⁷ is a strong indication that the surface is carbidic or oxycarbidic in nature (Supplementary Fig. 18b). In addition, a signal at 284.5 eV associated with graphitic carbon,⁴³ and peaks at 285.9 and 288.1 eV corresponding to oxidized carbon entities (C–O⁴⁸ and C=O respectively) are also visible in the spectrum. As seen from Supplementary Fig. 19, maintaining the catalyst under H₂ flow at 593 K decreased the oxide layer on the surface, but did not completely eliminate it. Specifically, the amount of Mo²⁺ increased by ca. 10% after 3 h under H₂ flow, and appeared to remain relatively constant at this value thereafter. As such, a 3 h pre-reduction was performed before the HDO reaction. The invariance in amount of Mo²⁺ after 3 h suggests that the remaining oxide layer (corresponding to Mo⁴⁺, Mo⁵⁺ and Mo⁶⁺ species) on the carbide is likely more difficult to be removed under these mild reduction conditions, consistent with prior reports wherein temperatures above 823 K was required to remove residual oxygen from fresh Mo₂C catalysts.²⁹

Micro-GC results. Benzene was the major HDO product observed over both MoO₃ (Supplementary Fig. 20) and Mo₂C (Supplementary Fig. 21). However, the rates of benzene formation were very different. Upon introduction of the H₂-anisole saturated stream over pre-reduced MoO₃, the benzene concentration increased sharply to reach a maximum in ca. 1.3 h, before very slowly decreasing over the next 6.7 h (Supplementary Fig. 20). In contrast, the benzene concentration reached a maximum in just ca. 0.4 h over Mo₂C, before dropping rapidly in the next 2.5 h (Supplementary Fig. 21). Benzene content continued to decrease thereafter, albeit at a slower rate. The presence of two deactivation profiles over Mo₂C is also consistent with observations from anisole HDO experiments performed at 593 K and atmospheric H₂ pressures over bulk and supported Mo₂C (Supplementary Figs. 22, 23). Notably, Mo₂C generated almost an order of magnitude more benzene than MoO₃, thereby suggesting that although both catalysts produced benzene, Mo₂C was significantly more active than MoO₃ under similar reaction conditions. We note that while Mo₂C (~25 m²/g) has a higher BET surface area than MoO₃ (~5 m²/g) before reaction, Delporte *et al.* showed that the surface area of MoO₃ increased from 4 m²/g to 150 m²/g over 15 hours in the presence of either H₂ or H₂/hydrocarbon mixture at 623 K.⁴⁹ Our catalyst likely undergoes a similar increase in surface in the presence of H₂/anisole mixture, although the extent of such increase is uncertain because the total pressure employed was significantly lower (1 mbar). Normalizing the rate by the pre-reaction surface area (i.e., a higher bound for MoO₃) still indicated that Mo₂C is a more active HDO catalyst than MoO₃. Minor products typically observed

during anisole HDO at 593 K and 1.013 bar of H₂ over MoO₃, such as phenol, cresols, toluene and methane, were not observed during NAP-XPS experiments (P_{H₂} < 0.001 bar).¹⁵ Since the H₂ pressure employed in this study is 3 orders of magnitude lower than that used under typical reactivity studies, the generation of these minor products probably falls under the detection limit of the micro-GC detector. As expected, benzene was the dominant product over Mo₂C, consistent with the high benzene selectivity (≥94% selectivity on C₆⁺ basis) observed during anisole HDO at 593 K, 1 bar H₂ pressure. This value is slightly higher than that observed by Bhan and co-workers during anisole HDO at 150°C^{26, 27} and this difference can be attributed to the absence of cyclohexane formed from the sequential hydrogenation of benzene at 593 K. Thermodynamic calculations show that benzene hydrogenation to cyclohexane is unfavourable (ΔG_{reaction} = +16.69 kJ/Mol) at 593 K (see Supplementary Table 11).^{50, 51} However, since no cyclohexane was detected, the calculated approach to equilibrium (see Supplementary Table 11) was likely much smaller than 1, thus indicating that benzene hydrogenation was not thermodynamically limited but likely kinetically controlled.^{26, 51} This low hydrogenation rate suggests suppressed hydrogenation activity of the oxygen-modified Mo₂C catalyst, as previously observed in the presence of oxygenated reactants such as anisole and other lignin-derived aromatics.^{26, 28} Direct HDO of anisole over Mo₂C typically yields benzene and methanol, with the latter undergoing further HDO to form methane and water.²⁶ However, no peaks corresponding to methane or methanol were observed in this study, likely due to the low amounts produced that approached the detection limit of the micro-GC (10 ppm).

Powder X-ray Diffraction (PXRD). PXRD patterns of pre-reduced MoO₃ showed that the bulk MoO₃ structure was preserved during the 3 h H₂ pretreatment (Supplementary Fig. 24). Similarly, the PXRD pattern of fresh Mo₂C showed only peaks associated with β-Mo₂C, with no visible diffractions from MoO₂ (see Supplementary Fig. 25). PXRD patterns of spent MoO₃ catalysts did not show any appreciable changes in the bulk MoO₃ structure (Supplementary Fig. 26). No new peaks corresponding to the MoO_xC_yH_z or MoO₂ were observed, contrasting to the PXRD patterns observed after HDO of m-cresol at 593 K.¹⁵ This can be attributed to the significantly lower H₂ pressure employed here which might not be high enough to cause a bulk transformation of the catalyst. While bulk oxycarbide was not observed after reaction, the increased presence of Mo⁵⁺ observed at the surface is indicative of surface oxycarbide formation (*vide infra*), consistent with our previous studies.¹⁵ Similarly, PXRD patterns of spent Mo₂C catalysts (Supplementary Fig. 27) reveal that the bulk structure of Mo₂C was preserved during HDO reaction, in agreement with prior observations by Bhan.²⁶

Discussion

Mo 3d spectra acquired during HDO of anisole over pre-reduced MoO₃ across both replicate experiments featured an initial oxidation phase (~4 h) followed by a reduction phase, before approaching a steady state composition. Effectively, the catalyst underwent an initial transient

oxidation-reduction cycle to move closer to its working state, as seen by the relatively constant distribution of Mo species towards the end of the experiment. During the initial stages of the reaction, the anisole feed oxidized the Mo⁵⁺ surface species to Mo⁶⁺ species, even at the high H₂-anisole molar ratios (~215) used. Similarly, the proportion of Mo⁴⁺ first increased, thus implying that some Mo sites were over-reduced to Mo⁴⁺ during the pre-reduction, before reaching a steady value of ca. 8%. This smaller proportion of Mo⁴⁺ on the surface compared to the Mo⁵⁺ or Mo⁶⁺ states indicates that Mo⁴⁺ does not play a significant role in HDO. We note that the amount of Mo⁴⁺ observed during these experiments was significantly lower than that observed in our prior work (49% Mo⁴⁺),¹⁶ likely due to the slower rate of reduction at the lower H₂ pressures used in the NAP-XPS chamber. We also note that no oxidation was observed in control experiments with MoO₃ in the absence of feed (anisole), thereby ruling out any significant oxygen contamination in the chamber. Since the oxidation was only observed upon introduction of feed, it is likely a direct effect from the interaction of the oxygenate with the catalyst surface. Once the feed is introduced, oxygen from the anisole can bind favourably to the undercoordinated Mo sites (Mo⁵⁺), thereby oxidizing the Mo species. This result is in line with observations by Delporte *et al.* wherein carbon atoms from the reactant rapidly fill oxygen vacancies to form an oxycarbohydride phase, thereby preventing the formation of MoO₂.⁴⁹ Similarly, our previous work also revealed that pre-reduced MoO₃ transformed into a mixture of MoO_xC_yH_z and MoO₂ after coming into contact with m-cresol for 0.5 h.¹⁵ In this study, oxidation continued up to ~ 4 h, at which point the catalyst transitioned to its working state with an equilibrated ratio of Mo⁶⁺/Mo⁵⁺ and steady state HDO rates. This oxidation-reduction cycle could possibly depict the actual turnovers observed on the MoO₃ catalytic surface. Taken together, the interplay of Mo⁵⁺ and Mo⁶⁺ states is strong evidence that Mo⁵⁺ is active for HDO under these reaction conditions. Furthermore, Mo 3d spectra acquired at higher photon energies of 946 eV and 1486.7 eV (see Supplementary Figs. 28-30) revealed that the surface of MoO₃ featured more Mo⁵⁺ and less Mo⁶⁺ states than the bulk, thus further confirming that Mo⁵⁺ is the active site responsible for HDO over MoO₃. Adsorption of oxygenates onto such undercoordinated Mo sites is also consistent with mechanisms proposed during HDO of acrolein⁵² and acetaldehyde⁵³ over MoO₃. Similarly, the same depth profile analysis (Supplementary Figs. 29,30) showed that the bulk was more enriched with Mo⁴⁺ states than the surface and that the amount of Mo⁴⁺ in bulk increased during reaction, indicating bulk-like over-reduction i.e. transport of oxygen vacancies propagating down to the bulk. This observation is also consistent with the rapid deactivation observed over MoO₃ at 673 K during HDO of m-cresol, attributed to the complete bulk-reduction of MoO₃ to MoO₂ (Mo⁴⁺),¹⁵ indicating that Mo⁴⁺ is not that active for HDO.

Analysis of the Mo 3d spectra of Mo₂C revealed that the dominant Mo²⁺ phase was maintained throughout the reaction, showing negligible oxidation even in the presence of the oxygenate feed. We note that the H₂ pre-reduction, as expected, led to an initial increase in the Mo²⁺ content (from 72% to 83%) and a corresponding

decrease in the oxide overlayer thickness (0.33 nm to 0.20 nm, see Supplementary Table 6). However, both the composition of Mo oxidation states and the oxygen coverage did not vary significantly during the HDO reaction, similar to that reported by Schaidle *et al.* during HDO of acetic acid over Mo₂C.⁵⁴ The prevalence of Mo²⁺ species and the negligible changes in Mo⁵⁺/Mo⁶⁺ oxidation states imply that the dominant carbide/oxycarbide phase is likely responsible for HDO over Mo₂C. This presence of oxycarbide phase during HDO was also illustrated by Schaidle *et al.* using DFT calculations, wherein a submonolayer of oxygen was shown to exist on the Mo-Mo₂C(001) and C-Mo₂C(001) surfaces during HDO of acetic acid.⁵⁴ Using a combination of *in situ* diffuse reflectance infrared Fourier transform spectroscopy (DRIFTS), temperature-programmed desorption of ammonia (NH₃-TPD) and DFT calculations, a 0.50 monolayer O/C-Mo₂C(001) was proposed to be the likely active catalyst surface under the reaction conditions investigated in their study.⁵⁴

Based on Mo₂C's nearly invariant Mo 3d spectra, *in situ* oxidation probably cannot account for the observed catalyst deactivation. Bhan and co-workers attributed catalyst deactivation both to mild coke formation and *in situ* oxidation.²⁷ If *in situ* oxidation were a major cause of deactivation, the proportion of higher Mo oxidation states (i.e. Mo⁴⁺, Mo⁵⁺ and Mo⁶⁺) would have increased with a concurrent decrease in the presence of Mo²⁺ species. Furthermore, XPS of spent supported Mo₂C catalysts (performed using an air-free transfer vessel with UHV XPS) after HDO of anisole at 593 K, 1 bar H₂ also revealed that the dominant Mo²⁺ state was maintained during the reaction even after 24 h with no appreciable surface oxidation (Supplementary Fig. 31), thereby excluding *in situ* oxidation as a cause for the observed deactivation even for atmospheric H₂ experiments. However, the O 1s spectra featured a signal at ca. 532.7 eV (Supplementary Figs. 32, 33) that can be attributed to the oxygen present in anisole-derived reaction intermediates or to methoxy species on the catalyst surface.^{26, 55} The signal increased during the reaction, implying growing oxygenate adsorption and potentially leading to deactivation by blocking some of the sites. Although this increase is also consistent with the oxygen incorporation reported by Bhan,²⁷ it seems to be a minor effect since it did not change the relative ratio of Mo oxidation states or the O/Mo ratios (Supplementary Figs. 34, 35) as reported in Schaidle's study.⁵⁴ It is possible that the rates of oxygen incorporation and surface reduction could have reached equilibrium, thereby leading to minimal changes on the quantity of O on the surface measured by XPS. This result is in agreement with prior reports wherein *in situ* oxidation predominantly occurred during the transient phase of HDO and that no further oxygen incorporation was observed during steady state HDO.²⁷ Similarly, since 'fresh' Mo₂C already had some oxygen on the surface prior to reaction (ca. 0.20 nm oxide overlayer), only minute amounts of oxygen were likely incorporated during the reaction. Hence, although *in situ* oxidation cannot be excluded as a cause for deactivation observed in this study, it likely plays only a minor role in the overall decrease in catalyst performance.

The role of coking in catalyst deactivation was investigated by analysing the C 1s spectra, the surface ele-

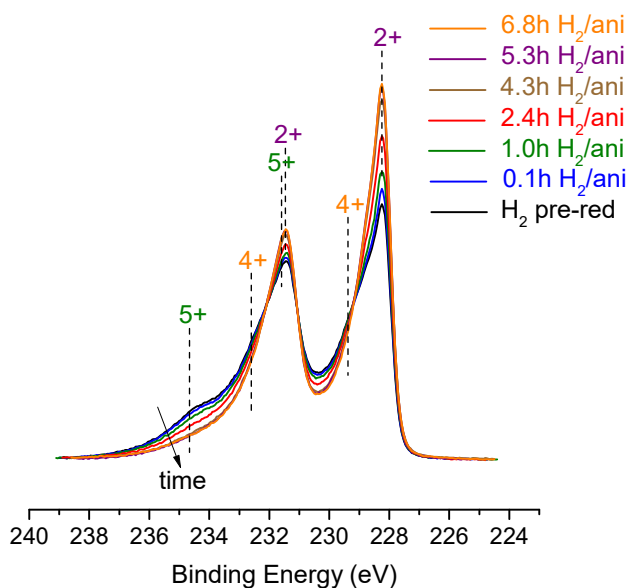


Fig. 3 | Normalized Mo 3d spectra of passivated Mo₂C (Mo₂C-pass) during HDO of anisole measured at photon energy of 473 eV. Reaction conditions: T = 593 K, P_{total} = 1 mbar (P_{anisole} = 0.005 mbar, balance H₂) and H₂ pre-reduction = 3 h

mental composition and the C/Mo atomic ratios. The time-resolved C 1s spectra and the composition of different C 1s components showed no significant changes (Supplementary Figs. 37-39), suggesting that the nature of the surface carbon species was largely invariant throughout the reaction. However, surface elemental quantification (Supplementary Methods IV) revealed that C content increased by ~6% (Supplementary Fig. 40). Similarly, the atomic C/Mo ratio as measured by XPS (Supplementary Fig. 41) increased by ca. 14%, indicating a growing amount of carbonaceous deposits on the surface during the course of reaction. The rise in both surface concentration of atomic carbon and C-Mo ratios across duplicate experiments (Supplementary Figs. 42-44) is in agreement with the observations by Bhan *et al.*²⁷ and Schaidle *et al.*⁵⁴ Taken together, these data are strong evidence that coking is likely the major cause of deactivation route for Mo₂C under the reaction conditions investigated here.

In order to understand the effect of an oxygen overlayer on the carbide surface on the HDO reactivity, a passivated carbide (Mo₂C-pass) was investigated under identical reaction conditions. The passivation oxide overlayer on Mo₂C-pass was determined to be approximately 1.34 nm, roughly 4 times thicker than that observed over fresh Mo₂C. High Mo oxidation states dominated the Mo 3d spectra of Mo₂C-pass (Supplementary Fig. 45), with only a small contribution from Mo²⁺ (20% of the Mo surface species), which is significantly lower than that for fresh Mo₂C (72%). The C 1s spectrum shows a carbidic signal at 283.2 eV, albeit less intense than that observed with fresh Mo₂C (Supplementary Fig. 46). The signals at 285.9 and 288.1 eV, associated with oxidized carbon are stronger than those of fresh Mo₂C. Supplementary Figure 47 shows that the passivated layer gets partially reduced during the H₂ treatment, as seen by an increase in the fraction of Mo²⁺ from 20% to 55% and a corresponding

decrease in oxygen coverage to a ca. 0.57 nm oxide overlayer or roughly 1.8 monolayers (based on a Mo-O bond distance of 0.318 nm⁵⁶), similar to the 1.3 monolayers observed by Bhan on a passivated Mo₂C catalyst after H₂ treatment.²⁷

The anisole feed did not further oxidize the Mo species on Mo₂C-pass (see Fig. 3). In fact, the oxide layer continued to decrease in intensity during the reaction. Supplementary Figure 48 shows that the combined proportion of Mo⁴⁺, Mo⁵⁺ and Mo⁶⁺ decreased from ca. 45% to 27% during reaction in the first 4 h, while the amount of Mo²⁺ concurrently increased from ca. 55% to 73%. The composition of Mo species was relatively constant after this 4 h time period, analogous to the trend observed with fresh Mo₂C. Similarly, the oxygen coverage further decreased to 0.27 nm oxide overlayer, approaching the oxygen coverage values observed over fresh Mo₂C after HDO reaction. Interestingly, although Mo₂C-pass sample showed similar amounts of reactivity towards benzene production (Supplementary Fig. 49) compared to fresh Mo₂C, this material also generated small quantities of toluene. This alkylation product is typically observed on bulk MoO₃^{14, 15} and is also a minor alkylation product observed on H₂-activated passivated Mo₂C during HDO of anisole.²⁶ The presence of toluene indicates that the surface of the passivated Mo₂C features Brønsted acidity,⁵¹ consistent with previous reports.^{54, 57} The presence of acid sites on Mo₂C is dependent on many factors such as carburization conditions, passivation treatment, oxygen removal efficiency during H₂ pre-reduction, and the presence of oxygen co-feed or any other oxygenates during reaction. Sullivan *et al.* used 2,6-di-tert-butylpyridine titrations to reveal that Brønsted acid sites were responsible for the dehydration of isopropanol (IPA) to propylene over an oxygen-modified Mo₂C and that these acid site densities can be reversibly tuned by a factor of ~ 30 using an O₂ co-feed.⁵⁸ Furthermore, Badour *et al.* showed that the proportion of acid sites can be tuned by the phase/composition of Mo₂C while the acid strength itself can be varied by the carbide particle size.⁵⁹ In summary, acid sites can be either found inherently on Mo₂C or can be formed either during pre-treatment or during reaction. However, the significance of these acid sites with respect to controlling reactivity is reaction-dependent. In the reaction investigated in our study, since anisole does not have a sp³-hybridized β-hydrogen, it cannot undergo dehydration, thus leading to deoxygenation mechanisms different from those observed during dehydration in the above-mentioned studies. The O 1s and C 1s spectra, as well as the elemental surface composition of carbon and atomic C-Mo ratios also showed similar trends to those observed with fresh Mo₂C (Supplementary Figs. 50-53). Mo₂C-pass featured a single deactivation regime (Supplementary Fig. 49), in comparison to the two deactivation zones observed over fresh Mo₂C. Overall, these differences in reactivity over fresh and passivated Mo₂C can be explained by the different amounts of initial oxides present on their surfaces. Specifically, the formation of toluene suggests that when the carbide passivation layer is thicker, the sites on the surface behave more like those in the bulk oxide material. Although toluene production in this study was under the detection limit due to the lower HDO reactivity

of MoO₃ at these conditions, alkylation activity has been reported for bulk and supported MoO₃ catalysts when operating at higher reactant partial pressures.

Though NAP-XPS showed that both MoO₃ and Mo₂C had surface oxycarbide (Mo_xO_yC_z) features, the oxycarbide observed over MoO₃ was significantly richer in oxygen than that on the surface of Mo₂C. As shown in Fig. 1, the Mo oxidation states observed for oxycarbide present on MoO₃ transitions between +6 and +5 oxidation states during reaction. In contrast, the oxycarbide over Mo₂C shows almost no +6 or +5 oxidation states and ca. 15% +4 oxidation state without change in the course of HDO (Fig. 2). This stark difference implies that the active sites of the two catalysts must be different. In addition to the differences in oxygen content, the electronic structure of the oxycarbide is altered by the MoO₃ or Mo₂C underlayer, in turn affecting the HDO activity. Differences in the surface composition of the catalysts will manifest as differences in reactivity, selectivity and catalyst stability.

In order to verify these differences, HDO experiments of 4-methylanisole were performed in flow reactors over Mo₂C and MoO₃ catalysts supported on silica (see Supplementary Methods V). Supported catalysts were used for these studies to mitigate differences in surface areas generated from formation of the oxycarbide phase. HDO performed with Mo₂C/SiO₂ at 5 bar H₂ and 623 K resulted in complete conversion of 4-methylanisole with a selectivity to toluene of ca. 90%, consistent with the high benzene selectivity observed in the HDO of anisole (see Supplementary Fig. 55). Under identical reaction conditions and similar space velocities, MoO₃/SiO₂ converted 15% of 4-methylanisole with an initial selectivity to toluene of ca. 80% that reduced to ca. 60% after 14 h, and remained constant at this value thereafter (Supplementary Fig. 56). Additionally, a combined selectivity to oxygenates, comprising mostly p-cresol, dimethylanisole and dimethylphenol at steady state of approximately 30% was observed. The presence of dimethylanisole and dimethylphenol also confirmed the presence of Brønsted acid sites capable of catalysing alkylation. In contrast, negligible transalkylation activity was observed for Mo₂C, consistent with the high selectivity to C–O bond cleavage and minimal alkylation observed in previous reports.^{26–28} Comparing MoO₃ with Mo₂C, it is apparent that oxycarbide generated from Mo₂C is more reactive and selective for HDO than the oxycarbide on MoO₃ under identical reaction conditions.

Mo₂C also showed excellent stability as it maintained 40% of its initial activity even after 140 h time on stream (Supplementary Fig. 55). The deactivation profiles obtained across two experiments were identical with first order deactivation rate constants of 0.017 h⁻¹. We hypothesize that the higher H₂ pressures employed in these experiments both reduced the formation of carbonaceous deposits and aided in the faster removal of coke already formed on the catalyst surface. To investigate this hypothesis, a series of reactions were performed over fresh Mo₂C catalyst where the H₂ pressure was varied over 1 to 6 bar (Supplementary Fig. 57). The first order deactivation rate constants were plotted against the average methane selectivity for the respective reaction conditions (see Supplementary Fig. 58). Lower deactivation rate constant is cor-

related with higher methane selectivity, implying that larger amounts of carbonaceous deposits are removed as methane at higher H₂ pressures, thereby significantly increasing catalyst stability. This deactivation mode is consistent with the higher C–Mo ratios observed by NAP-XPS over the carbide material during reaction.

In summary, both MoO₃ and Mo₂C are both promising HDO catalysts, capable of converting biomass-based oxygenate molecules to more valuable fuels and chemicals. Both catalysts were investigated for HDO of anisole at 1 mbar, 593 K while XPS spectra of Mo 3d, O 1s and C 1s were concurrently measured. MoO₃ and Mo₂C produced benzene as the main product of HDO. Mo 3d spectra for pre-reduced MoO₃ show that Mo⁵⁺ initially gets oxidized to Mo⁶⁺, followed by reduction to regenerate Mo⁵⁺ during the course of HDO reaction. In contrast, the Mo 3d spectra of fresh Mo₂C revealed that the dominant carbide phase (Mo²⁺) was retained throughout the HDO reaction, with no significant changes in the distribution of surface Mo species, which also included a small proportion of surface oxide species (ca. 0.20 nm overlayer). The carbide materials appeared to deactivate mainly via coking. An experiment with passivated Mo₂C (Mo₂C-pass) generated toluene in addition to benzene, demonstrating that the presence of oxide moieties generate acid sites sufficiently strong to promote alkylation.

Overall, our findings are largely consistent with the observations of Bhan and co-workers, wherein the dominant carbide phase is associated with a highly selective HDO product. While the surface of fresh Mo₂C is predominantly carbidic in nature (~85% Mo²⁺) throughout the reaction, it still has some oxidic character (~15% total of Mo⁴⁺, Mo⁵⁺ and Mo⁶⁺). This observation suggests that high HDO selectivity over Mo₂C can be attributed to some adsorbed oxygen on the Mo₂C surface,²⁶ resulting in the formation of just benzene from anisole. Taken together, NAP-XPS experiments over Mo₂C and passivated Mo₂C reveal that surface oxygen is likely necessary for selective HDO but too much surface oxygen makes the catalyst behave more like MoO₃, resulting in the production of alkylation side products. Hence, controlling surface oxygen concentration on the surface oxycarbide phase is critical for controlling HDO reactivity and product selectivity.

Methods

Preparation of materials. Anisole (99 %) was used as the reactant, and purchased from VWR International. Bulk MoO₃ (≥99.5%) and molybdenum oxide (MoO₂, ≥99 %) were purchased from Sigma-Aldrich. Bulk MoO₃ was pre-reduced for 3 h at 593 K, 1.013 bar under a H₂ flow (70 ml/min) to generate undercoordinated sites and remove the induction period reported in our previous study.¹⁵ Pre-reduced MoO₃ was transferred to the glovebox and sealed in a vial to prevent any oxidation. Fresh Mo₂C was synthesized from ammonium paramolybdate tetra (para)hydrate ((NH₄)₆Mo₇O₂₄·4H₂O, 99%, Alfa Aesar) using a temperature programmed reaction method. Ammonium paramolybdate was loaded into a ¼ inch U-tube reactor, dispersed on top of a quartz wool plug, in contact with a K-type thermocouple (Omega, model TJ36-CAXL-u6u). The reactor was then placed in a furnace

(Carbolite, model GTF 11/50/750B), connected to a temperature controller (Digi-Sense, model 68900-10). Ammonium paramolybdate tetra (para)hydrate was heated in a 21% CH₄-H₂ mixture (70 ml/min total flow) from room temperature to 923 K at 3 K/min and held at 923 K for 1 hour. The resulting sample (Mo₂C) was then held under pure H₂ flow (55 ml/min) at 923 K for another hour to scavenge residual surface carbon. The sample was cooled down under H₂ flow to room temperature. This U-tube reactor was equipped with valves for isolation of the catalyst, to prevent any exposure to air. Once room temperature was reached, the U-tube was then transferred to a nitrogen-filled glove box and the resulting Mo₂C catalyst was transferred to a 5 ml borosilicate glass ampule (Wheaton) and capped with a septum. These ampules were then evacuated on a Schlenk line outside of the glovebox, before being flame sealed. Passivated Mo₂C (Mo₂C-pass) was prepared under similar carburization conditions in a tube furnace, before being passivated with 1% O₂-N₂ mixture for 2 h and then being exposed to ambient atmosphere.

Powder X-ray Diffraction (PXRD). PXRD was performed on a Bruker D8 diffractometer using Nickel-filtered Cu-K α radiation ($\lambda = 1.5418 \text{ \AA}$). PXRD patterns were acquired on a 2D image plate, rotated at 15 rpm for 2θ values ranging from 20° to 90° with a step size of 0.04° and a scan speed of 0.2 s per step.

Near Ambient Pressure X-ray Photoelectron Spectroscopy (NAP-XPS) Experiments. NAP-XPS experiments were performed at the ISSS end-station of the Bessy II synchrotron facility in Berlin, Germany.³² The set up consisted of a differentially pumped electrostatic lens system and a SPECS hemispherical electron analyser. Detailed explanation of the set up can be found elsewhere.³² To ensure equal surface sensitivity, Mo 3d, O 1s and C 1s core-level regions were recorded using selected photon energies such that ejected photoelectrons had similar kinetic energy (~245 eV) across the different elements. This kinetic energy corresponds to a 0.66 nm inelastic mean free path (IMFP) for Mo₂C and 0.78 nm for MoO₃ based on the NIST Electron IMFP Database.⁶⁰ Given that the information depth is roughly three times the IMFP value, ~95% of the ejected photoelectrons arise from a depth of ca. 2.0 and 2.3 nm, approximately the top 10 and 7 atomic layers of Mo₂C (Mo-C bond 0.206 nm)⁵⁶ and MoO₃ (Mo-O bond 0.318 nm)⁵⁶ respectively. The spot size was 300 μm x 100 μm and the beam was moved to a new spot on the catalyst pellet (*vide infra*) for every set of XPS spectra measurement to minimize beam-induced reduction of molybdenum species.⁴¹ XPS spectra were acquired in normal emission geometry with a pass energy of 20 eV and a step size of 0.05 eV for Mo 3d and 0.1 eV for C 1s and O 1s. At each time point, the elemental core level spectra were measured sequentially in this order: Mo 3d, C 1s and O 1s. For each elemental core level, typically 5-8 scans were recorded. In total, the duration of spectrum acquisition for each elemental core level was ca. 5 min. All the XPS spectra shown in the manuscript and Supplementary Information correspond to the catalyst state measured at that

time point, with the time stamp referring to the start of Mo 3d core level spectra acquisition. Binding energies for each element were corrected using their respective second-order peak. After binding energy correction, the spectra were normalized and a Shirley background was applied.⁶¹ The spectra were then deconvoluted by least-square fitting of Gaussian-Lorentzian profiles using the software Plot,⁶² with exponential tail contributions added to account for the asymmetry in some of the peaks. Density functional theory (DFT) calculations were performed for metallic Mo, MoO₂ and Mo₂C to determine the joint density of states from which the theoretical XPS line shapes (see Supplementary Fig. 2) were generated to serve as references for the identification of the binding energies of the various constituent contributions for each compound (see Supplementary Table 1). Two sets of optimization parameters were determined based on analysing multiple spectra to best fit the MoO₃ and Mo₂C spectra (see Supplementary Tables 2-5 and Supplementary Figs. 3, 4). Then, the same set of parameters was used consistently across the MoO₃ and Mo₂C samples, respectively. The following constraints were used to determine the best optimization parameters: 1) spin-orbit splitting of 3.15-3.20 eV for Mo 3d_{5/2} and 3d_{3/2}, 2) area ratio of 3:2 for Mo 3d_{5/2}-Mo 3d_{3/2}, and 3) equal Gaussian-Lorentzian ratio for Mo 3d_{5/2}-Mo 3d_{3/2}. For quantitative elemental analysis, the raw areas for each element were integrated and then normalized by their respective photon flux and photoionization cross-sections and asymmetry parameters (see Supplementary Methods IV, Supplementary Tables 7-10 and Supplementary Fig. 5).

Pre-reduced MoO₃ and fresh Mo₂C catalyst powders were pressed into pellets (7 mm diameter) using a hand-held pellet press (Pike Technologies) in a nitrogen-filled glovebox. Fresh MoO₃, MoO₂ and passivated Mo₂C (Mo₂C-pass) were pelletized in ambient atmosphere. The catalyst pellet was then placed between two stainless steel plates, which were then mounted onto a sapphire plate, and secured with screws. Temperature was measured using a K-type thermocouple, which was wound around the screws, pressed firmly against the back plate, very close to the catalyst pellet. The air-sensitive pellets were moved from the glovebox to the NAP-XPS set up using a transfer vessel, which was then mounted directly onto the XPS set up, thereby minimizing air exposure. The sample was locally heated using laser irradiation of the unpolished back plate. All NAP-XPS experiments were typically run at 1 mbar. The gas flows and pressure of the reaction chamber were regulated using multiple mass flow controllers (MFCs, Bronkhorst) and motorized control valves. Anisole feed was introduced to the reaction chamber using a stainless steel saturator in the form of a H₂-anisole saturated stream. H₂ gas was initially saturated with anisole in the saturator at room temperature and at 1.013 bar using a MFC set at 30 ml/min. This corresponds to a H₂/anisole molar ratio of ~215. A part of this flow was delivered to the reaction chamber held at 1 mbar via a low ΔP MFC (17-20 ml/min). The rest of the saturated gas stream was directed to the vent. All catalyst samples were heated at 5 K/min from room temperature to 593 K, and maintained at 593 K throughout the experiments. MoO₃ and MoO₂ were heated in a N₂ flow (10 ml/min) while Mo₂C catalysts

were heated under a H₂ flow (10 ml/min), before switching to H₂-anisole mixture (17-20 ml/min) for all reactions at 593 K. During reaction, the gas phase composition was monitored using a 4-channel micro gas chromatograph (micro-GC, CP-4900, Varian Inc), equipped with thermal conductivity detectors. The micro-GC consists of 4 columns – 2 Molsieve 5 columns (10 m and 20 m), a PoraPLOT Q column (10 m) and an Al₂O₃/KCl column (10 m). The PoraPLOT Q (PPQ) column was predominantly used to track benzene and anisole. All the columns were held isothermal at the following temperatures: 2 Molsieve columns at 328 K and 315 K, PPQ column at 453 K and Al₂O₃/KCl column at 423 K. Each micro-GC run lasted for about 7.3 min, before the next injection was made. Typically, when no reactions were run, the anisole-saturated H₂ stream was injected into the micro-GC via a bypass line (10 ml/min). When the reaction was started, the H₂-anisole mixture was delivered to the reaction chamber, while the bypass was switched off. Similarly, at the end of each experiment, the H₂-anisole mixture was turned off and bypass was resumed. The bypass served as a baseline reference for the amount of benzene observed in the absence of reaction.

Data availability. All data are available from the corresponding author upon reasonable request.

References

1. Furimsky, E. Catalytic hydrodeoxygenation. *Appl. Catal., A* **199**, 147-190 (2000).
2. Huber, G.W., Iborra, S. & Corma, A. Synthesis of transportation fuels from biomass: chemistry, catalysts, and engineering. *Chem. Rev.* **106**, 4044-4098 (2006).
3. Choudhary, T. & Phillips, C. Renewable fuels via catalytic hydrodeoxygenation. *Appl. Catal., A* **397**, 1-12 (2011).
4. Bu, Q. et al. A review of catalytic hydrodeoxygenation of lignin-derived phenols from biomass pyrolysis. *Bioresour. Technol.* **124**, 470-477 (2012).
5. He, Z. & Wang, X. Hydrodeoxygenation of model compounds and catalytic systems for pyrolysis bio-oils upgrading. *Catal. Sustainable Energy* **1**, 28-52 (2012).
6. Ruddy, D.A. et al. Recent advances in heterogeneous catalysts for bio-oil upgrading via "ex situ catalytic fast pyrolysis": catalyst development through the study of model compounds. *Green Chem.* **16**, 454-490 (2014).
7. Tran, N., Uemura, Y., Chowdhury, S. & Ramli, A. A review of bio-oil upgrading by catalytic hydrodeoxygenation. *Appl. Mech. Mater.* **625**, 255-258 (2014).
8. Saidi, M. et al. Upgrading of lignin-derived bio-oils by catalytic hydrodeoxygenation. *Energy Environ. Sci.* **7**, 103-129 (2014).
9. Schutyser, W. et al. Influence of bio-based solvents on the catalytic reductive fractionation of birch wood. *Green Chem.* **17**, 5035-5045 (2015).
10. Anderson, E.M. et al. Reductive Catalytic Fractionation of Corn Stover Lignin. *ACS Sustainable Chem. Eng.* **4**, 6940-6950 (2016).
11. Anderson, E., Crisci, A., Murugappan, K. & Roman-Leshkov, Y. Bifunctional Molybdenum Polyoxometalates for the Combined Hydrodeoxygenation and Alkylation of Lignin-Derived Model Phenolics. *ChemSusChem* **10**, 2226-2234 (2017).
12. Venkatakrishnan, V.K., Delgass, W.N., Ribeiro, F.H. & Agrawal, R. Oxygen removal from intact biomass to produce liquid fuel range hydrocarbons via fast-hydrolysis and vapor-phase catalytic hydrodeoxygenation. *Green Chem.* **17**, 178-183 (2015).
13. Anderson, E.M. et al. Flowthrough Reductive Catalytic Fractionation of Biomass. *Joule* **1**, 613-622 (2017).
14. Prasomsri, T., Nimmanwudipong, T. & Román-Leshkov, Y. Effective hydrodeoxygenation of biomass-derived oxygenates into unsaturated hydrocarbons by MoO₃ using low H₂ pressures. *Energy Environ. Sci.* **6**, 1732-1738 (2013).
15. Prasomsri, T., Shetty, M., Murugappan, K. & Román-Leshkov, Y. Insights into the catalytic activity and surface modification of MoO₃ during the hydrodeoxygenation of lignin-derived model compounds into aromatic hydrocarbons under low hydrogen pressures. *Energy Environ. Sci.* **7**, 2660-2669 (2014).
16. Shetty, M., Murugappan, K., Prasomsri, T., Green, W.H. & Roman-Leshkov, Y. Reactivity and stability investigation of supported molybdenum oxide catalysts for the hydrodeoxygenation (HDO) of m-cresol. *J. Catal.* **331**, 86-97 (2015).
17. Murugappan, K. et al. Supported molybdenum oxides as effective catalysts for the catalytic fast pyrolysis of lignocellulosic biomass. *Green Chem.* **18**, 5548-5557 (2016).
18. Zhou, G., Jensen, P.A., Le, D.M., Knudsen, N.O. & Jensen, A.D. Atmospheric Hydrodeoxygenation of Biomass Fast Pyrolysis Vapor by MoO₃. *ACS Sustainable Chem. Eng.* **4**, 5432-5440 (2016).
19. Nolte, M.W., Zhang, J. & Shanks, B.H. Ex situ hydrodeoxygenation in biomass pyrolysis using molybdenum oxide and low pressure hydrogen. *Green Chem.* **18**, 134-138 (2016).
20. Shetty, M., Murugappan, K., Green, W.H. & Román-Leshkov, Y. Structural Properties and Reactivity Trends of Molybdenum Oxide Catalysts Supported on Zirconia for the Hydrodeoxygenation of Anisole. *ACS Sustainable Chem. Eng.* **5**, 5293-5301 (2017).
21. Ren, H. et al. Selective hydrodeoxygenation of biomass-derived oxygenates to unsaturated hydrocarbons using molybdenum carbide catalysts. *ChemSusChem* **6**, 798-801 (2013).
22. Lee, W.-S., Wang, Z., Zheng, W., Vlachos, D.G. & Bhan, A. Vapor phase hydrodeoxygenation of furfural to 2-methylfuran on molybdenum carbide catalysts. *Catal. Sci. Technol.* **4**, 2340-2352 (2014).
23. Xiong, K., Lee, W.S., Bhan, A. & Chen, J.G. Molybdenum Carbide as a Highly Selective Deoxygenation Catalyst for Converting Furfural to 2-Methylfuran. *ChemSusChem* **7**, 2146-2149 (2014).
24. Xiong, K., Yu, W. & Chen, J.G. Selective deoxygenation of aldehydes and alcohols on molybdenum carbide (Mo₂C) surfaces. *Appl. Surf. Sci.* **323**, 88-95 (2014).
25. McManus, J.R. & Vohs, J.M. Deoxygenation of glycolaldehyde and furfural on Mo₂C/Mo(100). *Surf. Sci.* **630**, 16-21 (2014).
26. Lee, W.-S., Wang, Z., Wu, R.J. & Bhan, A. Selective vapor-phase hydrodeoxygenation of anisole to benzene on molybdenum carbide catalysts. *J. Catal.* **319**, 44-53 (2014).
27. Lee, W.-S., Kumar, A., Wang, Z. & Bhan, A. Chemical Titration and Transient Kinetic Studies of Site Requirements in Mo₂C-Catalyzed Vapor Phase Anisole Hydrodeoxygenation. *ACS Catal.* **5**, 4104-4114 (2015).
28. Chen, C.-J., Lee, W.-S. & Bhan, A. Mo₂C catalyzed vapor phase hydrodeoxygenation of lignin-derived phenolic compound mixtures to aromatics under ambient pressure. *Appl. Catal., A* **510**, 42-48 (2016).
29. Chen, C.-J. & Bhan, A. Mo₂C Modification by CO₂, H₂O, and O₂: Effects of Oxygen Content and Oxygen Source on Rates and Selectivity of m-Cresol Hydrodeoxygenation. *ACS Catal.* **7**, 1113-1122 (2017).
30. He, S., Boom, J., van der Gaast, R. & Seshan, K. Hydrolysis of lignocellulosic biomass over alumina supported Platinum, Mo₂C and WC catalysts. *Front. Chem. Sci. Eng.* (2017).

31. Iida, T. et al. Encapsulation of molybdenum carbide nanoclusters inside zeolite micropores enables synergistic bifunctional catalysis for anisole hydrodeoxygenation. *ACS Catal.* **7**, 8147–8151 (2017).
32. Knop-Gericke, A. et al. X-Ray Photoelectron Spectroscopy for Investigation of Heterogeneous Catalytic Processes. *Adv. Catal.* **52**, 213–272 (2009).
33. Patt, J., Moon, D.J., Phillips, C. & Thompson, L. Molybdenum carbide catalysts for water–gas shift. *Catal. Lett.* **65**, 193–195 (2000).
34. Sullivan, M.M., Chen, C.-J. & Bhan, A. Catalytic deoxygenation on transition metal carbide catalysts. *Catal. Sci. Technol.* **6**, 602–616 (2016).
35. Choi, J.-S., Bugli, G. & Djéga-Mariadassou, G. Influence of the degree of carburization on the density of sites and hydrogenating activity of molybdenum carbides. *J. Catal.* **193**, 238–247 (2000).
36. Song, Z. et al. Molecular level study of the formation and the spread of MoO₃ on Au (111) by scanning tunneling microscopy and X-ray photoelectron spectroscopy. *J. Am. Chem. Soc.* **125**, 8059–8066 (2003).
37. Clayton, C. & Lu, Y. Electrochemical and XPS evidence of the aqueous formation of Mo₂O₃. *Surf. Interface Anal.* **14**, 66–70 (1989).
38. Marin-Flores, O., Scudiero, L. & Ha, S. X-ray diffraction and photoelectron spectroscopy studies of MoO₂ as catalyst for the partial oxidation of isooctane. *Surf. Sci.* **603**, 2327–2332 (2009).
39. Sian, T.S. & Reddy, G. Optical, structural and photoelectron spectroscopic studies on amorphous and crystalline molybdenum oxide thin films. *Sol. Energy Mater. Sol. Cells* **82**, 375–386 (2004).
40. Scanlon, D.O. et al. Theoretical and experimental study of the electronic structures of MoO₃ and MoO₂. *J. Phys. Chem. C* **114**, 4636–4645 (2010).
41. Baltrusaitis, J. et al. Generalized molybdenum oxide surface chemical state XPS determination via informed amorphous sample model. *Appl. Surf. Sci.* **326**, 151–161 (2015).
42. Frank, B., Cotter, T.P., Schuster, M.E., Schlögl, R. & Trunschke, A. Carbon dynamics on the molybdenum carbide surface during catalytic propane dehydrogenation. *Chemistry–A European Journal* **19**, 16938–16945 (2013).
43. Oshikawa, K., Nagai, M. & Orni, S. Characterization of molybdenum carbides for methane reforming by TPR, XRD, and XPS. *J. Phys. Chem. B* **105**, 9124–9131 (2001).
44. Ledoux, M.J., Huu, C.P., Guille, J. & Dunlop, H. Compared activities of platinum and high specific surface area Mo₂C and WC catalysts for reforming reactions: I. Catalyst activation and stabilization: Reaction of n-hexane. *J. Catal.* **134**, 383–398 (1992).
45. Óvári, L., Kiss, J., Farkas, A.P. & Solymosi, F. Reactivity of Mo₂C/Mo (100) toward oxygen: LEIS, AES, and XPS study. *Surf. Sci.* **566**, 1082–1086 (2004).
46. Clair, T.P.S. et al. Surface characterization of α-Mo₂C (0001). *Surf. Sci.* **426**, 187–198 (1999).
47. Sugihara, M., Ozawa, K.-i., Edamoto, K. & Otani, S. Photoelectron spectroscopy study of Mo₂C (0001). *Solid State Commun.* **121**, 1–5 (2001).
48. Gao, Q., Zhao, X., Xiao, Y., Zhao, D. & Cao, M. A mild route to mesoporous Mo₂C–C hybrid nanospheres for high performance lithium-ion batteries. *Nanoscale* **6**, 6151–6157 (2014).
49. Delporte, P., Pham-Huu, C., Vennegues, P., Ledoux, M.J. & Guille, J. Physical characterization of molybdenum oxycarbide catalyst; TEM, XRD and XPS. *Catal. Today* **23**, 251–267 (1995).
50. Janz, G.J. Thermodynamics of the Hydrogenation of Benzene. *J. Chem. Phys.* **22**, 751–752 (1954).
51. Baddour, F.G. et al. Late-Transition-Metal-Modified β-Mo₂C Catalysts for Enhanced Hydrogenation during Guaiacol Deoxygenation. *ACS Sustainable Chem. Eng.* **5**, 11433–11439 (2017).
52. Moberg, D.R., Thibodeau, T.J., Amar, F.G. & Frederick, B.G. Mechanism of hydrodeoxygenation of acrolein on a cluster model of MoO₃. *J. Phys. Chem. C* **114**, 13782–13795 (2010).
53. Mei, D., Karim, A.M. & Wang, Y. Density functional theory study of acetaldehyde hydrodeoxygenation on MoO₃. *J. Phys. Chem. C* **115**, 8155–8164 (2011).
54. Schaidle, J.A. et al. Experimental and computational investigation of acetic acid deoxygenation over oxophilic molybdenum carbide: surface chemistry and active site identity. *ACS Catal.* **6**, 1181–1197 (2016).
55. Liang, J. et al. Effective conversion of heteroatomic model compounds in microalgae-based bio-oils to hydrocarbons over β-Mo₂C/CNTs catalyst. *J. Mol. Catal. A: Chem.* **411**, 95–102 (2016).
56. Lee, J.S., Locatelli, S., Oyama, S. & Boudart, M. Molybdenum carbide catalysts 3. Turnover rates for the hydrogenolysis of n-butane. *J. Catal.* **125**, 157–170 (1990).
57. Bej, S.K., Bennett, C.A. & Thompson, L.T. Acid and base characteristics of molybdenum carbide catalysts. *Appl. Catal., A* **250**, 197–208 (2003).
58. Sullivan, M.M., Held, J.T. & Bhan, A. Structure and site evolution of molybdenum carbide catalysts upon exposure to oxygen. *J. Catal.* **326**, 82–91 (2015).
59. Baddour, F.G., Nash, C.P., Schaidle, J.A. & Ruddy, D.A. Synthesis of α-MoC_{1-x} Nanoparticles with a Surface-Modified SBA-15 Hard Template: Determination of Structure–Function Relationships in Acetic Acid Deoxygenation. *Angew. Chem. Int. Ed.* **55**, 9026–9029 (2016).
60. Powel, C. & Jablonski, A. NIST Electron Inelastic-Mean-Free-Path Database, Version 1.2, SRD 71. *National Institute of Standards and Technology, Gaithersburg, MD, USA* (2010).
61. Roiaz, M. et al. Reverse Water–Gas Shift or Sabatier Methanation on Ni (110)? Stable Surface Species at Near-Ambient Pressure. *J. Am. Chem. Soc.* **138**, 4146–4154 (2016).
62. Wesemann, M. & Thijsse, B.J. (*Plot version 0.997*; 2007).

Acknowledgements

This research was funded by BP through the MIT Energy Initiative Advanced Conversion Research Program and the National Science Foundation (award number 1454299). We thank Helmholtz-Zentrum Berlin for the allocation of synchrotron radiation beamtime at beamline ISSS of BESSY II. T. E. J. acknowledges the Alexander-von-Humboldt Foundation for financial support.

Author contributions

K.M. and Y.R. conceived the research ideas and designed the experiments. K.M. prepared the materials and performed PXRD. K.M., E.M.A., D.T. and K.S. performed the NAP-XPS experiments. K.M. and D.T. analysed the XPS data. T.E.J. performed DFT calculations. K.M. and Y.R. co-wrote the paper. Y.R. supervised the project. All authors discussed the results and commented on the different versions of the manuscript.

Competing interests

The authors declare no competing interest.

Additional information

Supplementary information is available for this paper at <https://doi.org/>

Reprints and permissions information is available at www.nature.com/reprints

Correspondence and requests for materials should be addressed to Y.R.

Publisher's note: Springer Nature remains neutral with regard to jurisdictional claims in published maps and institutional affiliations.